

A LOW MOMENTUM COMPACTION LATTICE FOR THE DIAMOND STORAGE RING

I.P.S. Martin^{1,2}, R. Bartolini^{1,2}, J. Rowland¹, B. Singh¹, C. Thomas¹

¹Diamond Light Source, Oxfordshire, UK

²John Adams Institute, University of Oxford, UK

Abstract

With the aim of generating short pulse radiation, a low momentum compaction lattice has recently been commissioned for the Diamond storage ring. By introducing both positive and negative dispersion in the bending magnets it has been possible to operate the storage ring in a quasi-isochronous state, resulting in a natural electron bunch length of less than 1 pico-second. A description of the techniques used to develop the lattice is given, along with first results obtained during recent machine trials. Operation with both positive and negative momentum compaction factor is also described.

INTRODUCTION

The generation of short pulse radiation is an active area of research for many laboratories. A source of such x-rays allows time-resolved science to be carried out in a number of areas, such as in imaging rapidly evolving systems or systems far from equilibrium. Whilst the most promising methods for generating ultra-short (femto-second or below) pulses of radiation are based on linear accelerator and free-electron laser technology, storage ring based methods can still make a valuable contribution to this field. To this end, a low momentum compaction factor (MCF) lattice has recently been commissioned for the Diamond storage ring, and the first dedicated user run took place at Easter this year.

THEORY

So called “low-alpha” lattices produce short x-ray pulses by directly compressing the longitudinal distribution of the circulating electrons (σ_l) by reducing the MCF. The electron bunch length is given by

$$\sigma_l = \frac{c\alpha}{2\pi f_s} \sigma_E \quad (1)$$

where α is the MCF, f_s is the synchrotron frequency and σ_E is the natural energy spread.

Controlling the MCF

The MCF is defined as the relative change in path length in one revolution of the storage ring with respect to the relative particle momentum deviation

$$\alpha = \frac{\Delta l / l_0}{\delta} \quad (2)$$

where $\delta = \Delta P / P_0$, P_0 is the nominal momentum and l_0 is the circumference. The MCF can be expanded as a function of δ in the following way

$$\alpha(\delta) = \alpha_1 + \alpha_2 \delta + \alpha_3 \delta^2 + O(\delta^3) \quad (3)$$

where the leading order terms are given by

$$\alpha_1 = \frac{1}{l_0} \oint_{l_0} \frac{\eta_1(s)}{\rho} ds \quad (4)$$

$$\alpha_2 = \frac{1}{l_0} \int_{l_0} \frac{\eta_1'(s)^2}{2} + \frac{\eta_2(s)}{\rho} ds$$

The first order MCF is determined by the dispersion in the bending magnets and can be minimised by focussing the beam such that the dispersion is both positive and negative in equal proportions inside the dipoles. The second order MCF consists of two terms; the first is fixed by the derivative of the dispersion around the ring, and the second term depends upon the second order dispersion in the bending magnets. This can in principle be adjusted using sextupole magnets to offset the first term and set α_2 to zero, a necessity in order to maintain adequate momentum aperture [1].

Longitudinal Beam Motion

In the absence of radiation damping and quantum fluctuations, the equations governing the longitudinal motion can be written as [1]:

$$\phi'(\delta) = h \left(\frac{\Delta \ell}{\ell} + \alpha_1 \delta + \alpha_2 \delta^2 + \alpha_3 \delta^3 \right) \quad (5)$$

$$\delta'(\varphi) = \frac{eV_{RF}}{2\pi E_0} [\sin(\varphi) - \sin(\varphi_s)]$$

where the term $\Delta \ell / \ell$ represents all momentum independent path lengthening effects from betatron oscillations, closed orbit errors or an RF frequency offset.

The longitudinal motion has stable and unstable fixed points which occur when both ϕ' and δ' are zero. The two phases at which the fixed points always occur are $\varphi = \varphi_s$ and $\varphi = \pi - \varphi_s$, and the momentum values for the fixed points are given by the roots of the equation

$$0 = \frac{\Delta \ell}{\ell} + \alpha_1 \delta + \alpha_2 \delta^2 + \alpha_3 \delta^3 \quad (6)$$

Under the assumption that all momentum-independent path lengthening effects have been corrected to zero, there exist three solutions to (6). For all the solutions to be real, the condition

$$\alpha_2^2 > 4\alpha_1\alpha_3 \quad (7)$$

must be satisfied. If this condition is broken then there exists only a single stable and a single unstable fixed

point, greatly increasing the available momentum aperture for the on-momentum bucket. This is demonstrated in the longitudinal phase space plots shown in Fig. 1. In the first plot α_1 and α_3 are of opposite sign resulting in 3 alpha-buckets enclosing stable motion. In the second plot the sign of α_1 and α_3 is the same and only a single RF bucket appears, leading to an increase in momentum aperture. For this reason, the low alpha lattice developed for the Diamond storage ring was chosen to have negative α_1 .

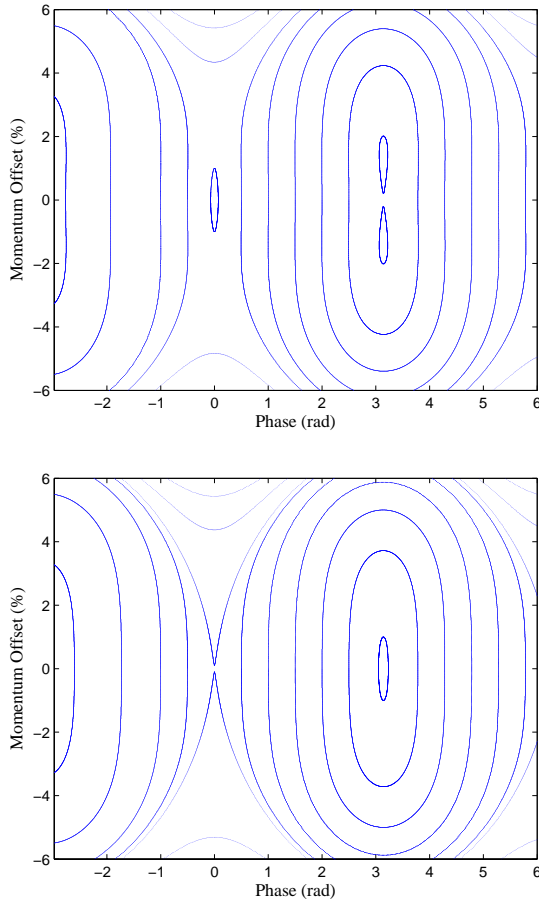


Figure 1: Longitudinal phase space plots: $\alpha_1=1.2\times 10^{-5}$, $\alpha_2=0$ and $\alpha_3=-6\times 10^{-6}$ (top); $\alpha_1=-1.2\times 10^{-5}$, $\alpha_2=0$ and $\alpha_3=-6\times 10^{-6}$ (bottom).

LATTICE DESCRIPTION

In order to identify a suitable tune region for low MCF operation, an objective function was constructed based on emittance, MCF, max beta function, etc. and minimised using simulated annealing. Two working regions were identified; the first was lower than the nominal betatron tune at $Q_x = 21$ compared to $Q_x = 27$, and gave a low MCF by introducing negative dispersion in the straight sections, with the dispersion crossing from positive to negative in the centre of the bending magnets. The second tune region was higher at $Q_x = 30$, and kept dispersion positive everywhere except for the very centre of the bending magnets. The second tune region had the added benefit of maintaining a low emittance of $\sim 3\text{-}4\text{nm}\cdot\text{rad}$. However, the higher natural chromaticity of this lattice

prevented a solution to be found with satisfactory dynamic aperture, and was abandoned in favour of the more relaxed low-tune solution. The main parameters of the final lattice are given in Table 1, and a plot of the Twiss parameters are given in Fig. 2.

Table 1: Main Low MCF Lattice Parameters

| Parameter | Value |
|--|--------------------------------|
| Emittance | 34.9 nm.rad |
| α_1 | -3×10^{-6} (variable) |
| α_2 (with/without sextupoles) | 0.0116 / -6.05×10^{-5} |
| α_3 | -4.25×10^{-2} |
| Tune point (Q_x / Q_y) | 21.150 / 12.397 |
| Natural Chromaticity (ξ_x / ξ_y) | -37.2 / -26.7 |
| $\beta_{x, ID} / \beta_{y, ID}$ | 8.24 m / 2.41 m |
| Natural bunch length (3.0MV) | 1.3 ps |
| Synchrotron frequency (3.0MV) | 346 Hz |

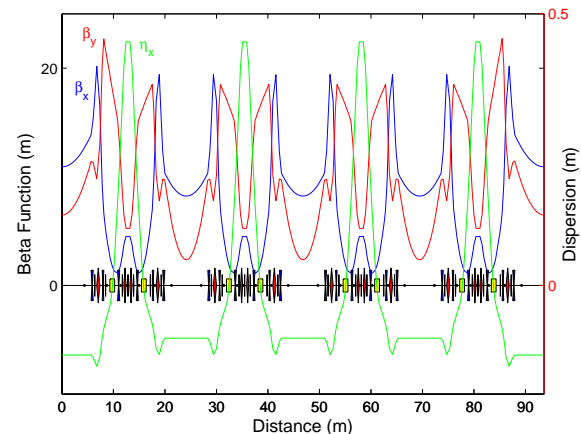


Figure 2: Twiss parameters for 1 super-period. A low MCF is achieved by varying the dispersion from positive to negative in the bending magnets.

MACHINE TRIALS

Machine trials began in September 2008, with first beam stored at $\alpha_1 = 1\times 10^{-5}$. Following a LOCO correction to the lattice [3], beta beat was reduced to the level of $\pm 10\%$, and the emittance and energy spread of the lattice confirmed from pinhole camera images. Following this initial setup, operation was switched to negative MCF.

Bunch Length Measurements

Bunch length measurements as a function of current are shown in Fig. 3 for several MCFs. In the limit of zero bunch current, the measured bunch lengths are in good agreement with those calculated from synchrotron tune measurements. At $\alpha_1 = -0.7\times 10^{-6}$, the measured bunch length approaches 1ps, an order of magnitude below what can be achieved in the nominal user lattice.

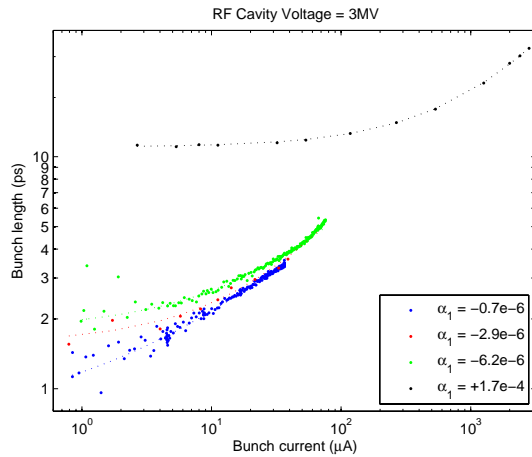


Figure 3: Bunch length vs. current for various MCFs. Values for the nominal user lattice are given for reference.

Transverse Beam Motion

Horizontal electron beam motion for the low MCF lattice has been measured to be greater than that of the nominal storage ring by up to two orders of magnitude. The beam motion is dominated by a dispersive pattern, implying the root cause of the increase in horizontal motion is related to fluctuations in the beam energy.

Shown in Fig. 4 are measurements of the horizontal electron beam displacement power spectral density (PSD) for 4 different values of the first order MCF. The profile of the vibrations remains constant in each case, with only the amplitude of motion and the location of the synchrotron frequency peak changing as the MCF is altered. The PSD profiles closely match the measured ground motion spectrum, suggesting that the primary mechanism driving the horizontal electron beam motion is small changes to the ring circumference ($<1\mu\text{m}$) caused by ground vibrations, rather than being directly driven by transverse quadrupole motion as in the nominal lattice. This follows directly from equation (2), which shows small changes to the ring circumference will directly translate into a change in the beam energy in inverse proportion to the MCF.

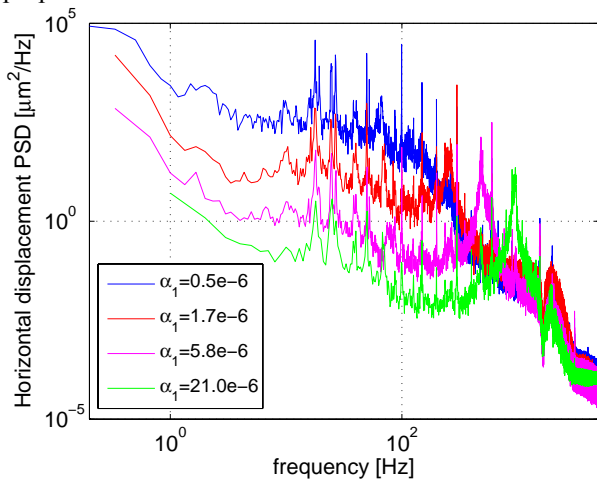


Figure 4: Displacement PSD at a high dispersion BPM for several values of the MCF.

In order to suppress transverse beam motion the fast orbit feedback (FOFB) has been set up to run with a reduced bandwidth. Integrated beam motion up to 1kHz is shown in Fig. 5 for the user setup given in Table 1. Whilst integrated horizontal beam motion in the range 1-100Hz is above that of the nominal lattice at $25\mu\text{m}$ compared to $2.5\mu\text{m}$, this is still well below the stability target of below 10% of beam size ($583\mu\text{m}$ at the BPM).

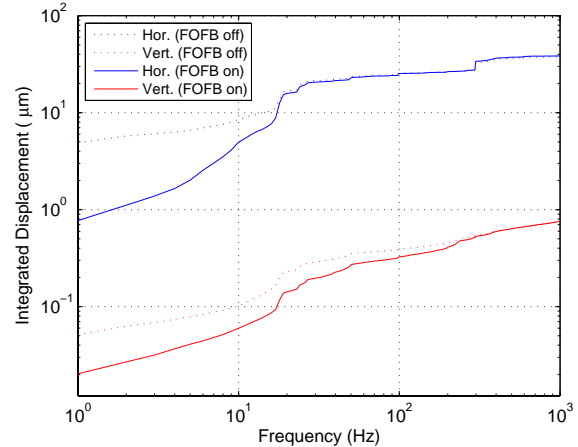


Figure 5: Integrated beam motion at a high dispersion BPM ($\eta_x = 0.45\text{m}$) with and without orbit feedback.

Operation with Positive MCF

In order to confirm the benefits of operating with negative MCF, tests were carried out at $\alpha_l = +1.1 \times 10^{-5}$. In this condition it was possible to store beam simultaneously at phases $\varphi = \varphi_s$ and $\varphi = \pi - \varphi_s$, as shown in Fig. 6 (cf. Fig. 1 top). In these conditions, lifetime for the on-momentum bucket was drastically reduced compared to similar conditions at negative MCF, and the range of RF frequencies over which beam could be stored was substantially lower.

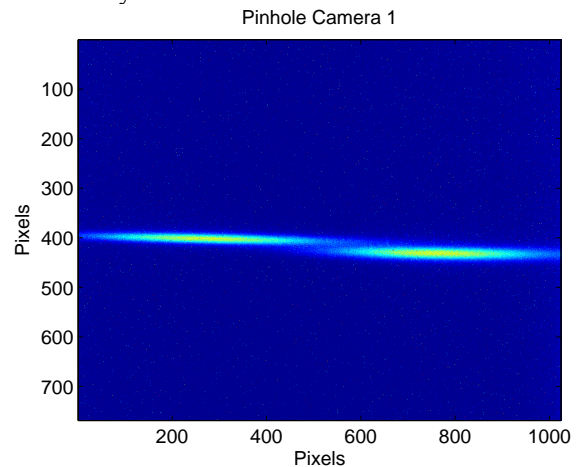


Figure 6: Pinhole camera image showing beam stored in 2 of the 3 alpha-buckets. Pixel size at source point: $2\mu\text{m}$.

REFERENCES

- [1] D. Robin et al. Phys. Rev. E 48 3 (1993)
- [2] Y. Shoji, PRST-AB 8, 094001 (2005)
- [3] J. Safranek, NIM A388, 27 (1997)